Expanding the Ge emission wavelength to 2.25 μm with Si_xN_y strain engineering

R.W. Millar,[1] K. Gallacher,[1] A. Samarelli,[1] J. Frigerio,[2] D. Chrastina,[2] T. Dieing,[3] G. Isella,[2] D.J. Paul[1*]

[1] University of Glasgow, School of Engineering, Rankine Building, Oakfield Avenue, Glasgow, G12 8LT, Scotland, United Kingdom

[2] L-NESS, Politecnico di Milano, Via Anzani 42, 22100, Como, Italy

[3] WITec Wissenschaftliche, Instrumente und Technologie GmbH, Lise-Meitner-Str. 6 D-89081 Ulm, Germany

***Corresponding Author:– Douglas.Paul@glasgow.ac.uk**

Abstract – Photoluminescence up to 2.25 μm wavelength is demonstrated from Ge nanopillars strained by silicon nitride stressor layers. Tensile biaxial equivalent strains of up to ~ 1.35% and ~ 0.9% are shown from 200 x 200 nm, and 300 x 300 nm square top Ge pillars respectively. Strain in the latter is confirmed by Raman spectroscopy, and supported by finite element modelling, which gives an insight into the strain distribution and its effect on the band structure, in pillar structures fully coated by silicon nitride stressor layers.

Introduction

Germanium has received significant attention as an optical material in recent years, as it has the potential to open the door to active, complementary metal-oxide semiconductor (CMOS) compatible, photonic components. Despite being an indirect bandgap material,

gain and lasing have been demonstrated from the Ge direct bandgap (Γ-band to heavy hole (HH) and light hole (LH)) [1][2], which is only ~140 meV above the indirect. This has come at the expense of high free carrier losses from degenerate n-type doping, which is required to move the Fermi level near to the Γ-band. Applying tensile strain to Ge has the potential to make it direct bandgap, as the Γ direct band energy decreases with strain at a greater rate than the indirect (L) [3], therefore creating a device which requires lower doping, and has a lower threshold. Furthermore, strained Ge photodiodes can have their absorption edge pushed to longer wavelengths, also resulting in enhanced absorption at 1.55 μm, and many other SiGe devices can be bandgap engineered by the application of external stress.

Several different methods of straining Ge have been demonstrated, including top down micro-bridge structures [4], nano-membranes [5,6], and high stress silicon nitride layers [7–10], which in particular have the advantage that they are fully CMOS compatible, and are already used for mobility enhancement of strained Si channels. Furthermore, silicon nitride (Si_xN_y – from here on referred to as SiN) stressors can alleviate the need for free standing structures, which can help reduce heating in optical devices. In this work, Ge nanopillars were fabricated to examine the limits of SiN stressors on small structures on Si substrates using fully CMOS compatible materials and processes. Results demonstrate emission up to 2.25 μm, which is a larger red shift than previously demonstrated using SiN stressor layers.

Growth

A low-energy plasma-enhanced chemical vapour deposition (LEPECVD) tool was used to grow 500 nm of Ge on a 100 mm diameter p-Si (100) wafer, as described in [11]. The Ge was in-situ phosphorus doped with $N_D \sim 2.5 \times 10^{19}$ cm^{-3} as confirmed by Hall-bar measurements at 300 K. In order to avoid out-diffusion of the phosphorus dopants [12], the wafer was not annealed, and therefore it has negligible strain in the Ge epilayer, which normally accumulates at high temperatures due to the difference in thermal expansion coefficients between Si and Ge. Raman spectroscopy confirmed the strain in the Ge epilayer was negligible. Photoluminescence measurements on blank samples demonstrated a direct band at 1.6 μm. This shift from ~1.55 μm (where the direct band is expected) is due to bandgap narrowing (BGN) from degenerate phosphorus doping [13]. Approximately 32 meV BGN has therefore been assumed to be constant over all strain levels, and taken into account when deducing strain levels from photoluminescence (PL) measurements.

Fabrication

Arrays of squares were patterned in hydrogen silsesquioxane (HSQ) resist, with separate arrays containing squares of 300 nm, and 200 nm side lengths. These were subsequently etched in a mixed SF_6 and C_4F_8 recipe [14] through the Ge epilayer and into the Si, leaving 560 nm tall pillar structures. Residual HSQ was removed in a buffered hydrofluoric acid solution.

An inductively coupled plasma, plasma enhanced chemical vapour deposition (ICP-PECVD) system was used to deposit layers of high stress silicon nitride (SiN). The stress in these layers was calculated by using a surface profiler to measure the curvature of a

silicon wafer before and after the silicon nitride deposition. This allows the stress in the film to be calculated using Stoney's equation [15]. This calculation also requires the film thickness of the SiN, which was measured by ellipsometry, and further verified by measuring the step height of a selectively stripped silicon nitride layer using a surface profiler.

Three separate samples were processed, each containing 300 and 200 nm square top pillars. One sample received a ~150 nm SiN layer with negligible stress, to be used as a reference. The other two samples received ~150 nm thick SiN layers with 1.9 GPa, and 2.7 GPa of compressive stress respectively. When deposited on patterned features, the compressive stress causes the SiN to expand, thus transferring tensile strain into the Ge features. 300 nm square top pillars with a SiN stressor layer is shown in Fig. 1.

Photoluminescence

Photoluminescence (PL) measurements were undertaken at room temperature on a Bruker Vertex 70 Fourier transform infrared (FTIR) spectroscopy system with an extended InGaAs detector with a cut-off at ~ 2.5 μm. The tool was operated in step-scan mode, which makes use of a lock in amplifier to discriminate against signals that have no frequency component with the 1 kHz optical chopper, which is placed in the beam path of the pump. The experimental setup is shown in Fig. 2, which shows the pump illuminating the sample through an aperture in a parabolic mirror. This mirror collects the sample emission, which is then coupled into internal interferometer of the FTIR system through a CaF_2 optical window. The step-scan measurement removes the ambient blackbody heating from the PL, which is normally visible in fast-scan operation. A diode

pumped, continuous wave solid-state laser emitting at 532 nm was used as the excitation source. In terms of energy, this corresponds to an excitation high above the Ge band-edge, so even at low excitation powers a small tail towards longer wavelengths is visible in the photoluminescence, which is the additional heating after the removal of the ambient blackbody. This can be observed in Fig. 3. The reference sample, with the negligibly stressed SiN layer, was used to confirm the absence of any optical effects such as diffraction that might alter the spectral shape of the emission. The sample stage was tilted through ~ 50° to confirm the spectra remained unchanged. Furthermore, it was confirmed that no heating was significant enough to move the Ge band-edge by varying the power of the pump with a neutral density filter. The shoulder in the PL from the reference sample at ~ 1.8 μm is from the Γ to HH transition.

As demonstrated in Fig. 3, the spectra were found to red-shift with increasing stress, and with decreasing size of the pillar. For the 300 nm pillars with 1.9 GPa stressors, only one peak is evident, which is thought to comprise emission from both the direct and indirect bands. With the increased stress of the 2.7 GPa stressor, a transition has moved to longer wavelengths, at close to 2 μm. This has been attributed to be the Γ to LH transition. At high levels of strain this transition is highly transverse magnetic (TM) polarised with the electric field parallel to the pillar axis [16], and therefore propagates parallel to the sample plane. This may account for the lack of intensity associated with this peak. Despite being highly polarized, however, a transverse electric (TE) component is still present, in part due to relaxation of the selection rules from non-parabolicity [17]. Furthermore, scattering processes will also serve to out-couple TM emission to the surface normal direction. Based on deformation potential theory [18], a Γ to LH transition

at this wavelength would suggest ~0.9 % biaxial equivalent strain in the 300 nm pillar, using deformation potential constants reported in [5]. This has been accounted for the 32 meV BGN measured on this material; a consideration that is important, as if neglected, it can otherwise overestimate the strain based on PL measurements.

For the 200 nm pillars, a reduction in intensity is observed compared to the 300 nm pillars. This is likely due to the reduced volume and therefore density of Ge material for a given area, as the same gap space was left between 300 and 200 nm pillars to allow for the lateral expansion of the SiN layers. Nevertheless, a clear red shift was still observable, with a peak centred at ~ 2.25 μm for the highest strain sample. This constitutes a redshift of 0.65 μm from the degenerately doped, unstrained band-edge, and is a larger redshift than other works using SiN stressor layers. Assuming Γ to LH transitions, this would result in up to ~ 1.35% biaxial equivalent tensile strain, when approximated using deformation potentials [5]. It is important to note that these strain levels are being compared to 'biaxial equivalent' strains, with regard to the energy (wavelength) of the Γ to LH transition.

Despite the pump being absorbed in the surface (< 20 nm) of the pillar, carrier diffusion should result in PL from the entire pillar [19]. This accounts for the small shoulder near 1.6 μm, and general broadening of the spectra in the 300 nm pillars (Fig. 3.), which is likely present due to strain gradients throughout the pillar structure. By comparison, the PL from the 200 nm pillars appears to be less broad, which could be interpreted as a sign of more uniform strain in the smaller structure. This is consistent with other works in the literature, which also demonstrate higher strain transfer into smaller structures, albeit

with larger then 1 μm features. Any physical effect, however, should still hold in nano-structures.

Raman Spectroscopy

In order to confirm the levels of strain in the pillars, Raman spectroscopy measurements were carried out on the highest strained samples, using a WITec Alpha 300 RAS spectrometer. For the backscatter geometry, this allows a measurement of the strain by determining how the longitudinal optical (LO) phonon frequency has changed compared to unstrained Ge [20]. The spatial resolution of the system was such that clear Lorentzian like peaks could be observed on the 300 nm pillars, but this was not found to be the case for the 200 nm pillars. The power of the focused 532 nm excitation source was reduced until heating was eliminated, which resulted in spectra close to the noise floor of the detector. Spectra from 200 nm pillars could not therefore be clearly interpreted and will be omitted. 300 nm pillars demonstrated some finite difference from pillar to pillar, which could further account from the broadening observed in the PL. Pillars with the highest strain, however, are expected to have enhanced radiative recombination efficiencies. The highest strained pillars in the sample scan area were fitted with a single Lorentzian, and found to have a Raman line at ~ 296.3 cm^{-1}, Fig. 4. If assuming purely biaxial strain, this can be used to calculate the strain using the relationship $\Delta\omega = b_{bi}\varepsilon_{bi}$, where $\Delta\omega$ is the change in frequency from the unstrained Raman line, b_{bi} is the strain shift coefficient ($= -424$ cm^{-1} [21]), and ε_{bi} is the biaxial strain.

Using phonon deformation potentials this therefore demonstrates a biaxial tensile strain of 0.91%, which is in good agreement with the PL. Deviation from biaxial strain,

however, can introduce error in these approximations, as the Raman line depends on all three components of the strain trace, i.e. ε_{xx}, ε_{yy}, and ε_{zz}, in the absence of shear stresses. Finite element modelling in Comsol Multiphysics was therefore used to model the strain distribution in a pillar. Given that some parameters were not known, such as the Young's modulus of the high stress SiN, the primary goal of the model was to understand the strain distribution, particularly with regard to the SiN on the pillar sidewalls. This is a particularly interesting comparison as other work has more commonly used just a top stressor. The Young's modulus was therefore estimated using a literature value for high stress SiN [8]. The elasticity tensor of Ge was included in the model, and orientated with the [100] direction aligned to the x-direction.

It was found that the inclusion of sidewall stressors, reduced the compression in the z-direction at the top plane, which is normally expected due to the tensile, in-plane strain from the top stressor through Poisson's ratio. Furthermore, tensile strain was found to be present in the z–direction away from the top plane. This increased the hydrostatic component has the effect of decreasing the Γ to L energy difference at a greater rate than purely biaxial strain, thus, becoming direct bandgap more quickly, Fig 5. Furthermore, the lateral expansion of the sidewalls, in the plane of each sidewall, appears to increase the x and y components of the strain in the top plane.

The strain tensor components were used to model the Raman line, down the centre of the 300 nm pillar structure, Fig 4. In the experiment, the volume contributing to the Raman line is that over the absorption depth of the source, with weighted contributions accounting for reabsorption of the Raman scattered signal. Therefore, corrections were

applied to the calculated Raman line [22], which resulted in a calculated value of 296.56 cm^{-1}, which is in good agreement with the measured value of 296.3 cm^{-1}.

Furthermore, the Γ to LH emission wavelength was calculated using deformation potentials, and accounting for BGN, which showed emission of 1.96 μm at the top plane. This again appears to be consistent with the experimental results. This was modelled for both cases of top stressors, and stressors deposited all around the pillar. The benefit of this type of strain distribution can clearly be understood in terms of the difference shown in Fig. 5. If this type of strain transfer can be applied to components that support an optical mode, it would be significantly advantageous, as reduced doping would be required in order to move the Fermi level to the Γ band, and as a result free carrier losses would be reduced.

Conclusion

Highly red-shifted emission from tensile strained Ge nanopillars has been demonstrated, showing biaxial equivalent Γ to LH emission of up to ~ 1.35 % in 200 nm nanopillars. This has been achieved through the application of high stress SiN layers to the nanopillar structures. Raman measurements confirm ~0.9 % biaxial equivalent strains in 300 nm pillars. Finite element modelling provides an insight into the effect of sidewall stressors in these geometries, highlighting that enhanced hydrostatic strain reduce the Γ to L-bands energy difference at greater rates than purely biaxial strain. Further work is required to incorporate this type of strain distribution into Ge cavity structures, to allow for the potential of Si compatible lasers and sources.

Acknowledgements

The authors would like to thank the staff of the James Watt Nanofabrication Centre for help with the fabrication. The work was funded by U.K. EPSRC (Project no. EP/H02364X/1) and EC GEMINI (Project No. 613055).

References

[1] J. Liu, X. Sun, R. Camacho-Aguilera, L. C. Kimerling, and J. Michel, Ge-on-Si laser operating at room temperature., Opt. Lett. 35 (2010) 679–81.

[2] R. E. Camacho-Aguilera, Y. Cai, N. Patel, J. T. Bessette, M. Romagnoli, L. C. Kimerling, and J. Michel, An electrically pumped germanium laser., Opt. Express. 20 (2012) 11316–20.

[3] D.J. Paul, Silicon photonics: a bright future?, Electron. Lett. 45 (2009) 582.

[4] M. J. Süess, R. Geiger, R. a. Minamisawa, G. Schiefler, J. Frigerio, D. Chrastina, G. Isella, R. Spolenak, J. Faist, and H. Sigg, Analysis of enhanced light emission from highly strained germanium microbridges, Nat. Photonics. 7 (2013) 466–472.

[5] J. R. Sánchez-Pérez, C. Boztug, F. Chen, F. F. Sudradjat, D. M. Paskiewicz, R. B. Jacobson, M. G. Lagally, and R. Paiella, Direct-bandgap light-emitting germanium in tensilely strained nanomembranes., Proc. Natl. Acad. Sci. U. S. A. 108 (2011) 18893–8.

[6] C. Boztug, J. R. Sánchez-Pérez, J. Yin, M. G. Lagally, and R. Paiella, Grating-coupled mid-infrared light emission from tensilely strained germanium nanomembranes, Appl. Phys. Lett. 103 (2013) 201114.

[7] G. Capellini, C. Reich, S. Guha, Y. Yamamoto, M. Lisker, M. Virgilio, A. Ghrib, M. El Kurdi, P. Boucaud, B. Tillack, and T. Schroeder, Tensile Ge microstructures for lasing fabricated by means of a silicon complementary metal- oxide-semiconductor process, Opt. Express. 22 (2014) 102–109.

[8] A. Ghrib, M. de Kersauson, M. El Kurdi, R. Jakomin, G. Beaudoin, S. Sauvage, G. Fishman, G. Ndong, M. Chaigneau, R. Ossikovski, I. Sagnes, and P. Boucaud, Control of tensile strain in germanium waveguides through silicon nitride layers, Appl. Phys. Lett. 100 (2012) 201104.

[9] A. Ghrib, M. El Kurdi, M. de Kersauson, M. Prost, S. Sauvage, X. Checoury, G. Beaudoin, I. Sagnes, and P. Boucaud, Tensile-strained germanium microdisks, Appl. Phys. Lett. 102 (2013) 221112.

[10] A. Ghrib, M. El Kurdi, M. Prost, S. Sauvage, X. Checoury, G. Beaudoin, M. Chaigneau, R. Ossikovski, I. Sagnes, and P. Boucaud, All-Around SiN Stressor for High and Homogeneous Tensile Strain in Germanium Microdisk Cavities, Adv. Opt. Mater. 3 (2015) 353–358.

[11] G. Isella, D. Chrastina, B. Rössner, T. Hackbarth, H.-J. Herzog, U. König, and H. von Känel, Low-energy plasma-enhanced chemical vapor deposition for strained Si and Ge heterostructures and devices, Solid. State. Electron. 48 (2004) 1317–1323.

[12] R. Geiger, J. Frigerio, M. J. Süess, D. Chrastina, G. Isella, R. Spolenak, J. Faist, and H. Sigg, Excess carrier lifetimes in Ge layers on Si, Appl. Phys. Lett. 104 (2014) 062106.

[13] R. Camacho-Aguilera, Z. Han, Y. Cai, L. C. Kimerling, and J. Michel, Direct band gap narrowing in highly doped Ge, Appl. Phys. Lett. 102 (2013) 152106.

[14] M. M. Mirza, H. Zhou, P. Velha, X. Li, K. E. Docherty, A. Samarelli, G. Ternent, and D. J. Paul, Nanofabrication of high aspect ratio (~50:1) sub-10 nm silicon nanowires using inductively coupled plasma etching, J. Vac. Sci. Technol. B Microelectron. Nanom. Struct. 30 (2012) 06FF02.

[15] G.G. Stoney, The Tension of Metallic Films Deposited by Electrolysis, Proc. R. Soc. A Math. Phys. Eng. Sci. 82 (1909) 172–175.

[16] D. S. Sukhdeo, S. Gupta, M. L. Brongersma, and K. C. Saraswat, Study of Carrier Statistics in Uniaxially Strained Ge for a Low-Threshold Ge Laser, IEEE J. Sel. Top. Quantum Electron. 20 (2014) 16–22.

[17] D.J. Paul, The progress towards terahertz quantum cascade lasers on silicon substrates, Laser Photon. Rev. 4 (2010) 610–632.

[18] E. Kasper, K. Lyutovich, Properties of Silicon Germanium and SiGe:Carbon, INSPEC, (2000).

[19] F. Pezzoli, F. Isa, G. Isella, C. V. Falub, T. Kreiliger, M. Salvalaglio, R. Bergamaschini, E. Grilli, M. Guzzi, H. von Känel, and L. Miglio, Ge Crystals on Si Show Their Light, Phys. Rev. Appl. 1 (2014) 044005.

[20] C.-Y. Peng, C.-F. Huang, Y.-C. Fu, Y.-H. Yang, C.-Y. Lai, S.-T. Chang, and C. W. Liu, Comprehensive study of the Raman shifts of strained silicon and germanium, J. Appl. Phys. 105 (2009) 083537.

[21] D. J. Lockwood and J. F. Young, Light Scattering in Semiconductor Structures and Superlattices, 273 (1991).

[22] I. De Wolf, H. E. Maes, and S. K. Jones, Stress measurements in silicon devices through Raman spectroscopy: Bridging the gap between theory and experiment, J. Appl. Phys. 79 (1996) 7148–7156.

Figure captions:

Figure 1:

A scanning electron microscope image of 300 x 300 nm square top Ge nanopillars, coated by ~150 nm of high stress SiN.

Figure 2:

Illustration showing the experimental setup used to measure photoluminescence spectra from the Ge nanopillars. The sample is illuminated through an aperture in a parabolic mirror.

Figure 3:

The photoluminescence from Ge nanopillars, coated with SiN layers of varying stress. The spectra have been scaled for clarity and therefore emission intensities should not be compared. The legend indicates pillar square top side length, and SiN stress respectively.

Figure 4:

a) The calculated Raman lines down the centre of 300 x 300 nm square top Ge nanopillars with 2.7 GPa stressors: a top only stressor (red) and a pillar fully coated by Si_xN_y (blue). The increased shift in the Raman line from the full stressor is due to an increased ε_{zz} component, with z being parallel to the height of the pillar.

b) The measured Raman lines of the unpatterned Ge epitaxial layer and of a strained 300 x 300 nm Ge pillar with a 2.7 GPa SiN stressor layer.

Figure 5:

Calculated Γ to L valley energy difference for cases of top only, and all over SiN stressors on a 300 nm Ge nanopillar. The inset shows an illustration indicating the line segment down which the calculation was made in the model.

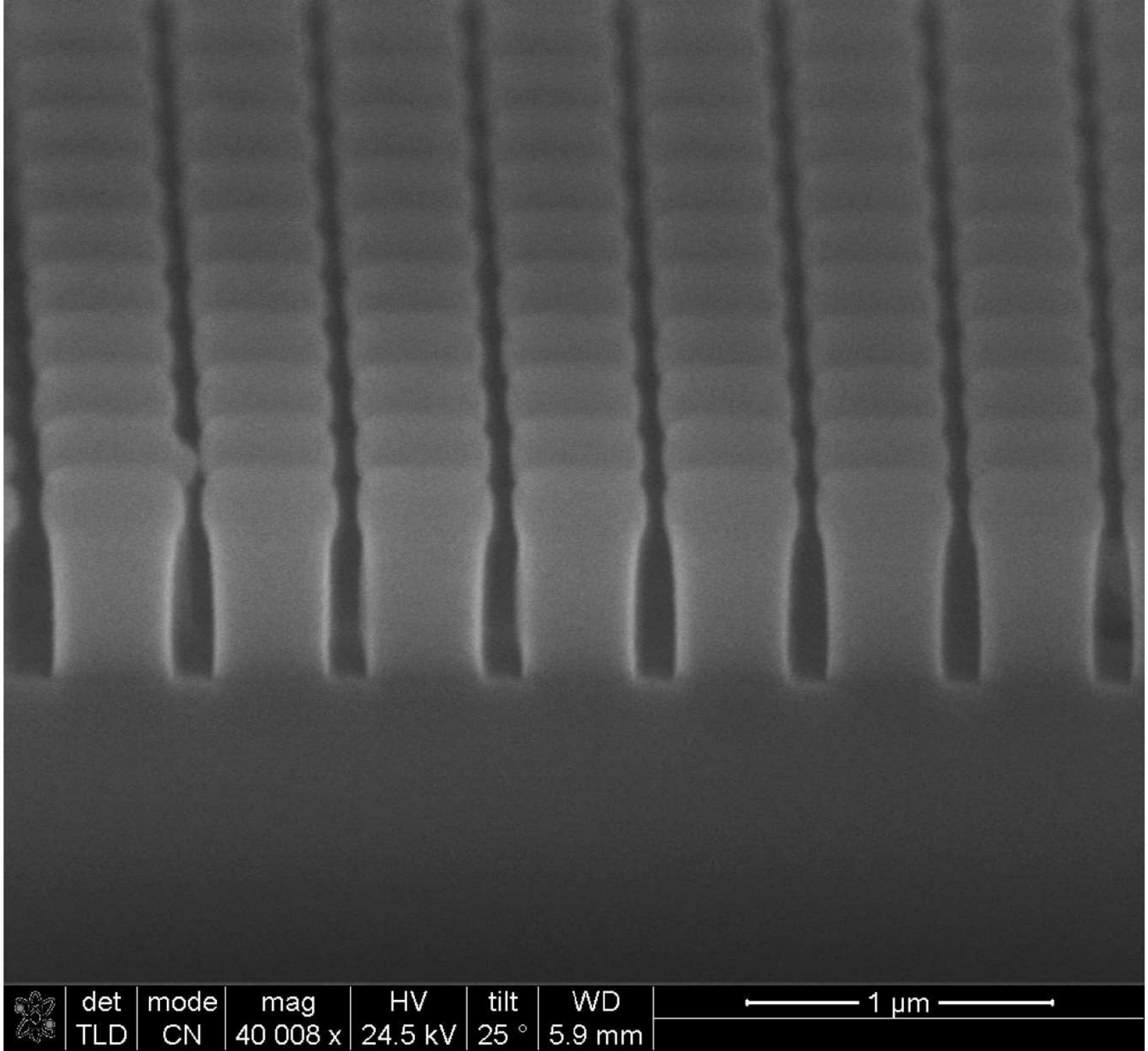
det
TLD
mode
CN
mag
40 008 x
HV
24.5 kV
tilt
25 °
WD
5.9 mm
1 µm

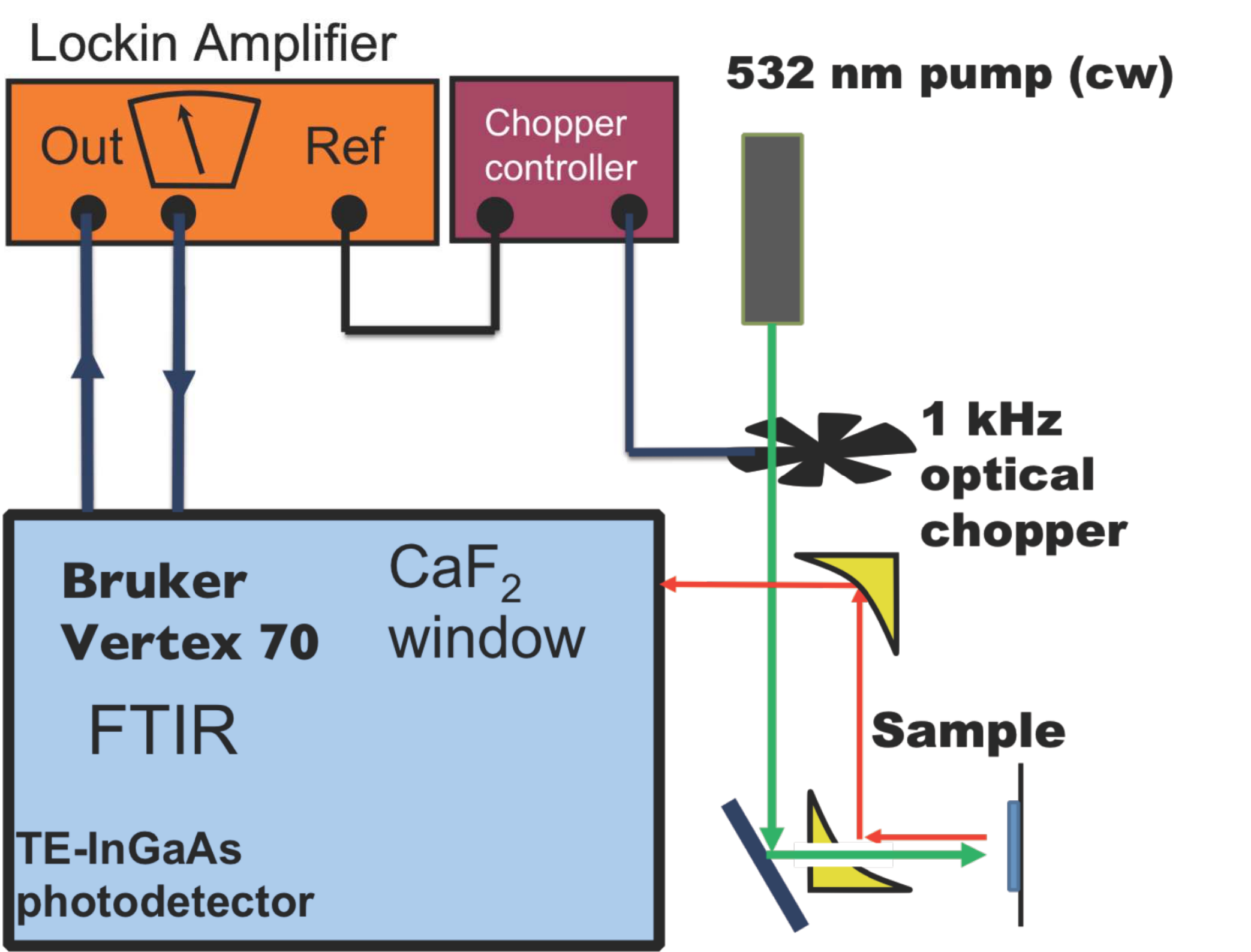
Lockin Amplifier
Out
Ref
Chopper controller
532 nm pump (cw)
1 kHz optical chopper
Bruker Vertex 70
FTIR
CaF2 window
TE-InGaAs photodetector
Sample

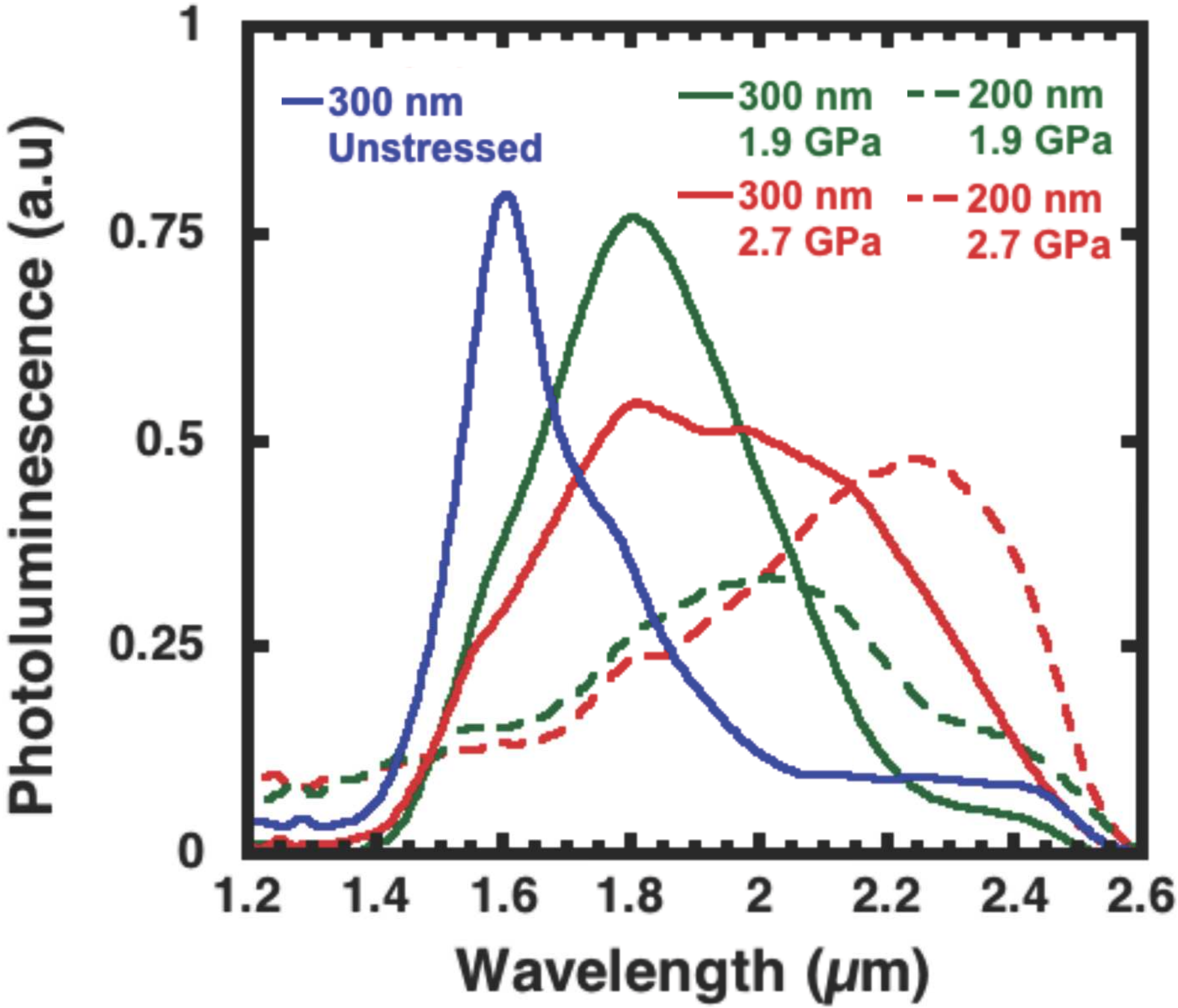
Photoluminescence (a.u)
1
0.75
0.5
0.25
0
1.2
1.4
1.6
1.8
2
2.2
2.4
2.6
Wavelength (μm)
300 nm
Unstressed
300 nm
1.9 GPa
200 nm
1.9 GPa
300 nm
2.7 GPa
200 nm
2.7 GPa

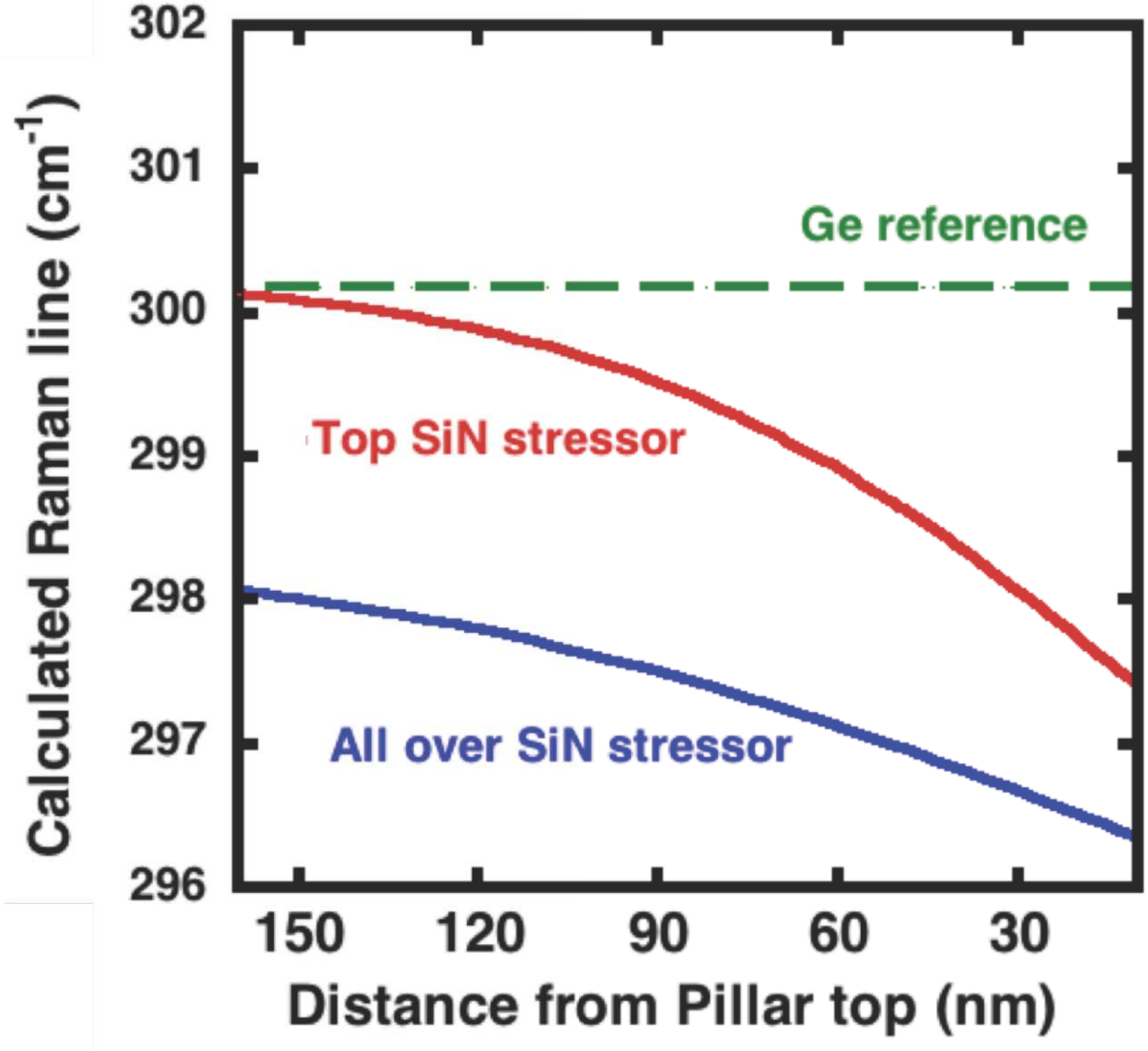
Calculated Raman line (cm-1)
302
301
300
299
298
297
296
Ge reference
Top SiN stressor
All over SiN stressor
150
120
90
60
30
Distance from Pillar top (nm)

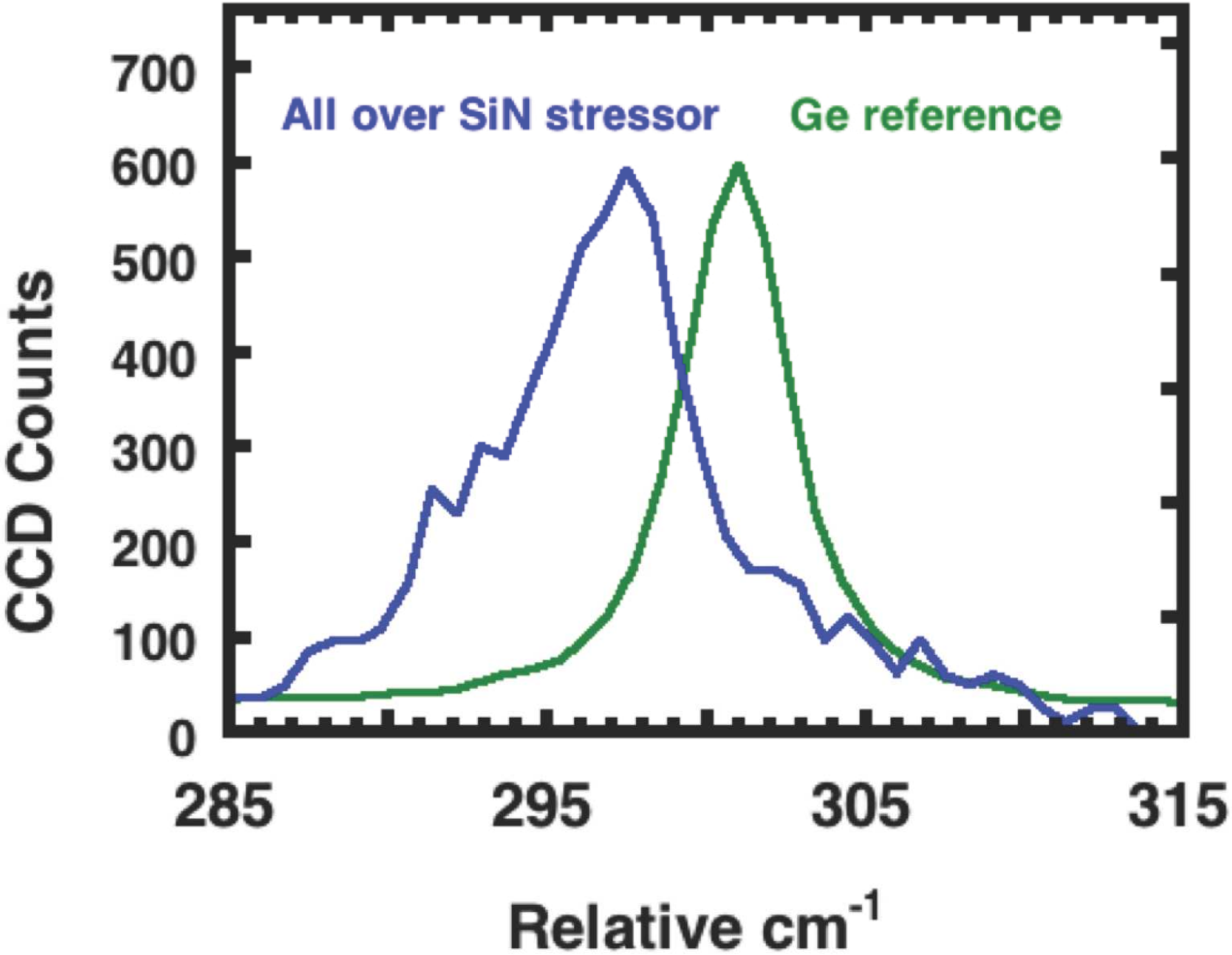
All over SiN stressor
Ge reference
CCD Counts
700
600
500
400
300
200
100
0
285
295
305
315
Relative cm-1

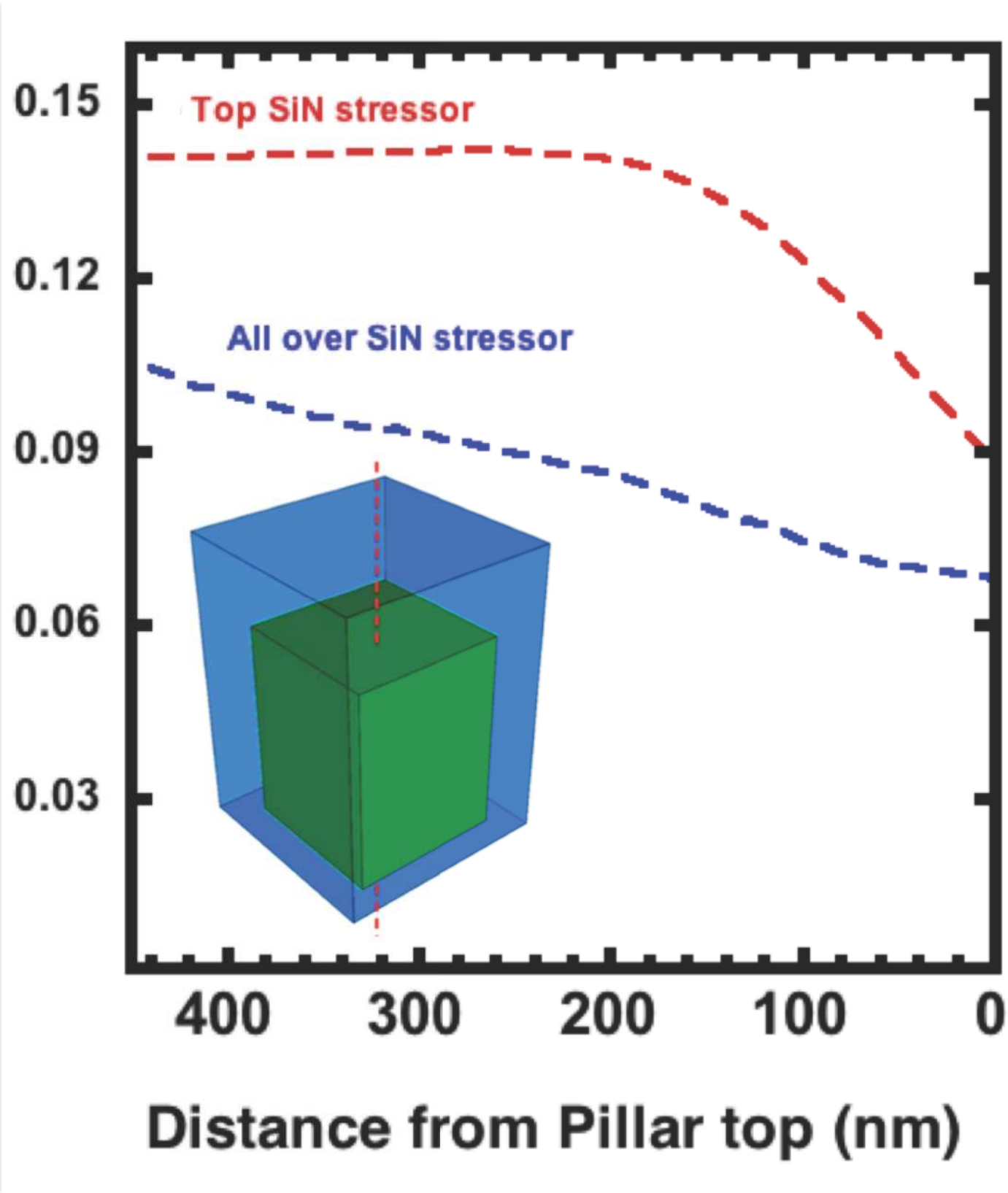
Top SiN stressor
All over SiN stressor
0.15
0.12
0.09
0.06
0.03
Γ to L energy (eV)
400
300
200
100
0
Distance from Pillar top (nm)